Journal of Peridynamics and Nonlocal Modeling (2023) 5:121–132
https://doi.org/10.1007/s42102-021-00068-9

ORIGINAL ARTICLES

The Variational Explanation of Poisson's Ratio in Bond-Based Peridynamics and Extension to Nonlinear Poisson's Ratio

Ekim Ekiz[1] · **Ali Javili**[1]

Received: 26 May 2021 / Accepted: 8 October 2021 / Published online: 24 November 2021

Abstract
It is commonly stated that the Poisson's ratio associated with bond-based peridynamics is $\frac{1}{4}$ for three-dimensional isotropic elasticity. This manuscript critically revisits this statement from a variational perspective for both two-dimensional and three-dimensional problems. To do so, a purely geometrical description of Poisson's ratio is considered. Unlike the commonly established treatment of the problem, the Poisson's ratio here is calculated via minimizing the internal energy density, rather than quantifying it and comparing it to its counterpart in classical linear elasticity. The advantage of the proposed approach is threefold. Firstly, elements of Cauchy linear elasticity such as "strain", "stress" and "elastic parameters" are entirely absent throughout the derivations here. This is particularly important since peridynamics is a non-local formulation, and therefore, using local notions such as "strain" and "stress" implies locality and is misleading. Secondly, unbound by linear elasticity, the proposed approach unlocks the limitation of the analysis to small deformations. Hence, it can be immediately applied to large deformations, resulting in a nonlinear Poisson's ratio that is no longer constant. Thirdly, the two-dimensional analysis here is purely two-dimensional, corresponding to a two-dimensional manifold in a three-dimensional space. That is, the two-dimensional formulation is neither plane stress nor plane strain that are rather degenerate three-dimensional cases. This contribution introduces the notion of nonlinear Poisson's ratio in peridynamics for the first time and proves that the nonlinear Poisson's ratio at the reference configuration coincides with $\frac{1}{4}$ for three-dimensional and $\frac{1}{3}$ for two-dimensional problems.

Keywords Bond-based Peridynamics · Nonlinear Poisson's ratio · Geometrically exact peridynamics

1 Introduction

Peridynamics (PD) established by Silling [1] is a non-local continuum mechanics theory, see also [2]. In PD, the behavior of each material point is dictated by its interactions with other material points in its vicinity. In contrast to classical continuum mechanics (CCM), the

✉ Ali Javili
ajavili@bilkent.edu.tr

[1] Department of Mechanical Engineering, Bilkent University, Ankara 06800, Turkey

integro-differential governing equations of PD are appropriate for problems involving discontinuities, immediately rendering PD suitable for fracture mechanics and related problems [3]. However, the range of PD applications is broad and not limited to fracture mechanics. Various applications and extensions of PD have been investigated in the past two decades. For a brief description of PD together with a review of its applications and related studies in different fields to date, see [4] and the references therein.

The original PD theory of Silling [1] was restricted to bond-based interactions. Bond-based peridynamics cannot capture a Poisson's ratio other than $\frac{1}{4}$ for isotropic three-dimensional (3D) elastic materials. This shortcoming was addressed in various contributions and rectified in [5, 6] via the introduction of the notion of state-based peridynamics. Also, recently CPD was established [7] as a geometrically exact formulation of PD whose underlying kinematics coincide with that of CCM. Despite the limitation of bond-based PD to capture Poisson's ratio, it is commonly employed to predict fracture and damage.

This manuscript aims (i) to elaborate on the notion of Poisson's ratio in bond-based PD and (ii) to introduce a nonlinear Poisson's ratio suitable for large deformations. The analysis here builds upon *minimizing the internal energy density* of the material, rather than quantifying it and comparing it with its counterpart in CCM linear elasticity. Therefore, the derivations are carried out through a variational structure entirely devoid of elements of classical linear elasticity such as *stress* and *strain*, or the constitutive tensor for that matter. This variational approach is where the current contribution parts ways with the commonly accepted description of the problem [8] further explored in [9]. The current view on the problem has two key advantages, as follows.

- Peridynamics, in principle, is a non-local formulation that may not rely on the gradient of the displacement field. Therefore, introducing a framework that discusses only displacements, rather than strains, is more in the spirit of PD. Here, Poisson's ratio ν is immediately identified without recourse to a strain-stress relationship, or other constitutive material parameters associated with CCM.
- In this framework, Poisson's ratio is a purely geometrical (dimensionless) parameter, independent of elastic constants. Unlike the common approach [8] that relies on CCM linear elasticity, the current proposition immediately offers a suitable method for large deformations too. This allows us to introduce a nonlinear Poisson's ratio for PD, for the first time.

2 Preliminaries

Central to our formulation is the geometrically exact description of the problem. Consider the deformation of a continuum body that occupies the material configuration $\mathcal{B}_0 \subset \mathbb{R}^3$ at time $t = 0$, and is mapped to the spatial configuration $\mathcal{B}_t \subset \mathbb{R}^3$ via the nonlinear deformation map †, as illustrated in Fig. 1. That is,

$$\boldsymbol{x} = \boldsymbol{y}(\boldsymbol{X}, t) \;\; : \;\; \mathcal{B}_0 \times \mathbb{R}_+ \to \mathcal{B}_t \,,$$

with $\boldsymbol{X}$ and $\boldsymbol{x}$ identifying points in the material and spatial configurations, respectively. The non-locality assumption of PD dictates that any point $\boldsymbol{X}$ in the material configuration can interact with other points within its finite neighborhood $\mathcal{H}_0(\boldsymbol{X})$, referred to as the material *horizon*. The *measure* of the horizon in the material configuration, denoted as δ, is generally the radius of a spherical neighborhood at $\boldsymbol{X}$. The horizons $\mathcal{H}_0$ and $\mathcal{H}_t$ coincide with the points $\boldsymbol{X}$ and $\boldsymbol{x}$ in the limit of an infinitesimal neighborhood. The neighbor set $\{\boldsymbol{X}^{\mathrm{I}}\}$ of the

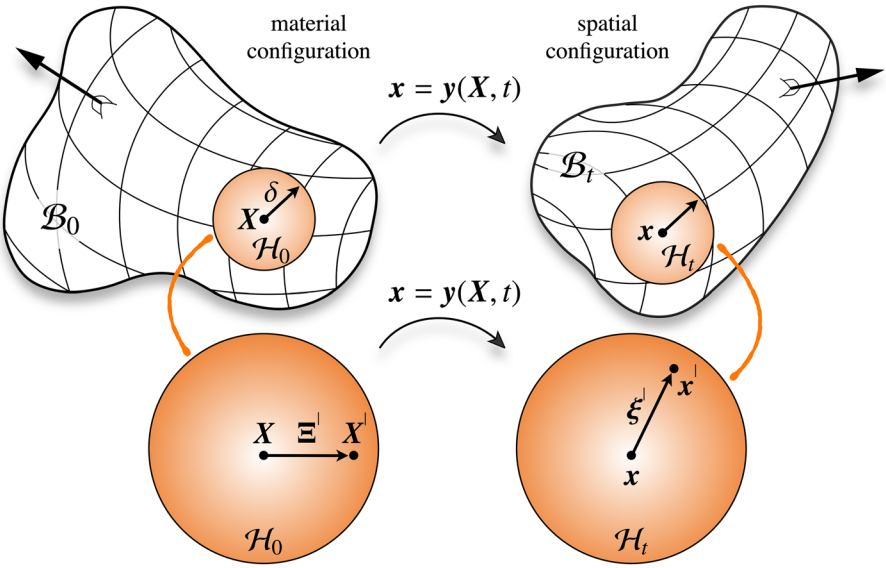

Fig. 1 Motion of a continuum body within the PD formulation. The continuum body that occupies the material configuration $\mathcal{B}_0 \subset \mathbb{R}^3$ at time $t = 0$ is mapped to the spatial configuration $\mathcal{B}_t \subset \mathbb{R}^3$ via the nonlinear deformation map $\boldsymbol{y}$. The neighborhood of $\boldsymbol{X}$ is mapped to the neighborhood of $\boldsymbol{x}$

point $\boldsymbol{X}$ includes all the neighbors $\boldsymbol{X}^{|}$ within the horizon. The neighbors $\boldsymbol{X}^{|}$ are mapped to their spatial counterparts via $\boldsymbol{y}$ as $\boldsymbol{x}^{|} = \boldsymbol{y}(\boldsymbol{X}^{|}, t)$. The relative positions between a point and its neighbors are denoted by $\boldsymbol{\Xi}^{|}$ and $\boldsymbol{\xi}^{|}$ in the material and spatial configurations, respectively. That is

$$\boldsymbol{\Xi}^{|} := \boldsymbol{X}^{|} - \boldsymbol{X} \quad , \qquad \boldsymbol{\xi}^{|} := \boldsymbol{x}^{|} - \boldsymbol{x} \, .$$

The bond stretch $S^{|}$ is defined by $S^{|} = l^{|}/L^{|}$ with $L^{|} := |\boldsymbol{\Xi}^{|}|$ and $l^{|} := |\boldsymbol{\xi}^{|}|$ where $L^{|}$ and $l^{|}$ are the bond lengths in the material and spatial configurations, respectively.

Let $T\mathcal{B}_0$ and $T\mathcal{B}_t$ denote tangents to the manifolds $\mathcal{B}_0$ and $\mathcal{B}_t$, respectively. For an affine deformation, with a linear deformation map $\boldsymbol{F}$ between the line elements $\mathrm{d}\,\boldsymbol{\Xi}^{|} \in T\mathcal{B}_0$ and $\mathrm{d}\,\boldsymbol{\xi}^{|} \in T\mathcal{B}_t$, the mapping reads

$$\mathrm{d}\,\boldsymbol{\xi}^{|} = \boldsymbol{F} \cdot \mathrm{d}\,\boldsymbol{\Xi}^{|} \, , \tag{1}$$

such that for an affine deformation $\boldsymbol{F}$ performs its natural obligation and thus

$$\text{affine deformation} \qquad \Rightarrow \qquad \boldsymbol{\xi}^{|} = \boldsymbol{F} \cdot \boldsymbol{\Xi}^{|} \, . \tag{2}$$

Of particular interest for this contribution is the deformation map $\boldsymbol{F}$ associated with a uniaxial tension test, illustrated in Fig. 2. With λ and η being the extensional and lateral stretches, respectively, $\boldsymbol{F} = \mathrm{Diag}(\lambda, \eta)$ for two-dimensional problems and $\boldsymbol{F} = \mathrm{Diag}(\lambda, \eta, \eta)$ for three-dimensional problems.

While Poisson's ratio usually corresponds to small strain linear elasticity, its definition can be cast into more generic forms suitable for finite deformations, too. The notion of a

nonlinear Poisson's ratio was suggested by Beatty and Stalnaker [10] for a simple extension as

$$\nu = -\frac{\text{lateral contraction}}{\text{longitudinal extension}} = -\frac{\eta - 1}{\lambda - 1} \qquad \Rightarrow \qquad \nu = \frac{1 - \eta}{\lambda - 1}\,. \tag{3}$$

The generic definition of Poisson's ratio (3) is suitable for small and large deformations. However, for large deformations various definitions for Poisson's ratio can be constructed. The commonly accepted measures [11, 12] for nonlinear Poisson's ratio of compressible elastic materials are

$$\begin{aligned}
&\text{Biot} \quad : \quad \nu = \frac{1-\eta}{\lambda-1} && \eta = 1 - \nu\,[\lambda - 1]\,,\\
&\text{Hencky} \quad : \quad \nu = -\frac{\ln \eta}{\ln \lambda} && \eta = \lambda^{-\nu}\,,\\
&\text{Green} \quad : \quad \nu = \frac{1-\eta^2}{\lambda^2-1} && \eta = \sqrt{1 - \nu\,[\lambda^2 - 1]}\,,\\
&\text{Almansi} \quad : \quad \nu = \frac{1-\eta^{-2}}{\lambda^{-2}-1} && \eta = \sqrt{\frac{1}{1 - \nu\,[\lambda^{-2} - 1]}}\,.
\end{aligned} \tag{4}$$

All the formats of nonlinear Poisson's ratio (4) coincide at infinitesimal deformations. The nonlinear Poisson's ratios (4) at $\lambda \to 1$ recover the classical Poisson's ratio associated with the small strain linear elasticity theory. This approach towards Poisson's ratio is crucial in the current contribution since its geometric nature is preserved and is introduced solely in terms of the stretches. As such, for a given λ and η, Poisson's ratio can be computed immediately without further connection to CCM, which is a key feature of the current approach. The remaining task therefore is to compute η for a prescribed λ that is elaborated next.

In order to compute η for a given λ, firstly η is expressed as $\eta = \eta(\nu;\lambda)$, given in Eq. (4). The semicolon is used to indicate that λ is a prescribed value but ν is a variable. Secondly, the internal energy density Ψ is expressed in terms of ν as $\Psi = \Psi(\nu;\lambda)$. Thirdly, to impose equilibrium, we set the variation of the internal energy density with respect to Poisson's ratio to zero. These three key steps are summarized as

$$\begin{aligned}
&\Psi = \Psi(\eta;\lambda) \quad \text{and} \quad \eta = \eta(\nu;\lambda) \quad \Rightarrow \quad \Psi = \Psi(\nu;\lambda) \quad \Rightarrow\\
&\delta\Psi = \frac{\partial \Psi}{\partial \nu}\,\delta\nu \doteq 0 \quad \Rightarrow \quad \frac{\partial \Psi}{\partial \nu} \doteq 0 \quad \Rightarrow \quad \nu \checkmark\,.
\end{aligned} \tag{5}$$

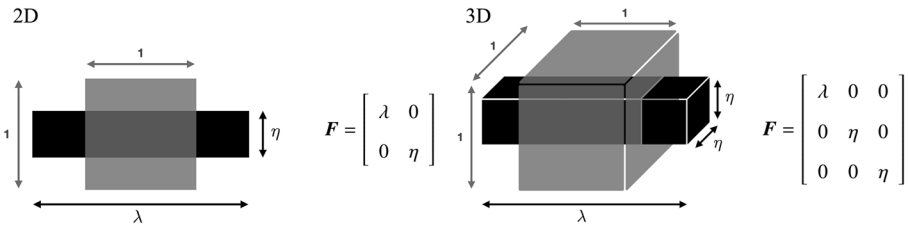

Fig. 2 Affine deformation of a unit domain via the linear deformation map $\boldsymbol{F}$ between the line elements $\mathrm{d}\,\boldsymbol{\Xi}^{\mathrm{I}} \in T\mathcal{B}_0$ and $\mathrm{d}\,\boldsymbol{\xi}^{\mathrm{I}} \in T\mathcal{B}_t$, for 2D (left) and 3D (right). The prescribed deformation represents a uniaxial tension test. Extensional and lateral stretches are denoted as λ and η, respectively

Note that the third step in particular is exactly where the current contribution differs from the commonly accepted approach to this problem [8, 9], where the authors compute Ψ itself and compare it with the internal energy density of Cauchy linear elasticity to identify the material parameters.

2.1 Two-Dimensional Formulation

For a two-dimensional domain, the internal energy density Ψ per unit *area* in the material configuration is the integral of its density $\psi^{\prime}$ over the horizon $\mathcal{H}_0$. That is, $\psi^{\prime}$ is the internal energy density per *area* squared in the material configuration as

$$\begin{aligned} \psi^{\prime} &= \frac{1}{2} C L^{\prime} [\, S^{\prime} - 1 \,]^2 \qquad \Rightarrow \\ \Psi &= \frac{1}{2} \int_{\mathcal{H}_0} \psi^{\prime} \, \mathrm{d} A^{\prime} \qquad \Rightarrow \\ \Psi &= \frac{1}{2} \int_{\mathcal{H}_0} \frac{1}{2} C L^{\prime} [\, S^{\prime} - 1 \,]^2 \, \mathrm{d} A^{\prime} \,. \end{aligned} \tag{6}$$

The bond-based interaction energy density $\psi^{\prime}$ is expressed as a harmonic potential with a bond constant C. Also, the factor one-half before the integral is introduced to prevent double-counting since the combination of each pair of points within the horizon occurs twice. Therefore, for the uniaxial tension test of interest here, the internal energy density Ψ reads

$$\Psi = \frac{1}{2} \int_{\mathcal{H}_0} \frac{1}{2} C \, |\boldsymbol{\Xi}^{\prime}| \, \Big[\, \frac{|\boldsymbol{F} \cdot \boldsymbol{\Xi}^{\prime}|}{|\boldsymbol{\Xi}^{\prime}|} - 1 \, \Big]^2 \, \mathrm{d} A^{\prime} \,. \tag{7}$$

It proves useful to decompose the bond vector $\boldsymbol{\Xi}^{\prime}$ into its magnitude $|\boldsymbol{\Xi}^{\prime}|$ and its direction $\hat{\boldsymbol{\Xi}}^{\prime}$ as

$$\boldsymbol{\Xi}^{\prime} = |\boldsymbol{\Xi}^{\prime}| \, \hat{\boldsymbol{\Xi}}^{\prime} \qquad \text{with} \qquad |\hat{\boldsymbol{\Xi}}^{\prime}| = 1 \,. \tag{8}$$

Therefore, the internal energy density (7) is expressed as

$$\Psi = \frac{1}{2} \int_{\mathcal{H}_0} \frac{1}{2} C \, |\boldsymbol{\Xi}^{\prime}| \, \Big[\, |\boldsymbol{F} \cdot \hat{\boldsymbol{\Xi}}^{\prime}| - 1 \, \Big]^2 \, \mathrm{d} A^{\prime} \qquad \text{with} \qquad \boldsymbol{F} = \mathrm{Diag}(\lambda, \eta) \,. \tag{9}$$

Note that Eq. (9) is nonlinear and therefore, λ and η need not be close to unity in Eq. (9). However, in order to show how the current proposition recovers the classical linear solution, we also provide its linearized version close to the reference configuration. Through linearization, given in 1, the internal energy density Ψ reads

$$\begin{aligned} &\Psi = \frac{1}{2} \int_{\mathcal{H}_0} \frac{1}{2} C \, |\boldsymbol{\Xi}^{\prime}| \, \Big[\, \boldsymbol{F} : [\hat{\boldsymbol{\Xi}}^{\prime} \otimes \hat{\boldsymbol{\Xi}}^{\prime}] - 1 \, \Big]^2 \, \mathrm{d} A^{\prime} \qquad \text{with} \\ &\boldsymbol{F} = \mathrm{Diag}(\lambda, \eta) \qquad \text{and} \qquad \{\lambda, \eta\} \approx 1 \,. \end{aligned} \tag{10}$$

Integrating Eq. (10) over the horizon using a polar coordinate system with $\mathrm{d} A^{\prime} = |\boldsymbol{\Xi}^{\prime}| \, \mathrm{d} \, |\boldsymbol{\Xi}^{\prime}| \, \mathrm{d} \, \Theta^{\prime}$ renders

$$\Psi = \frac{1}{2}\int_{\Theta^{|}=0}^{\Theta^{|}=2\pi}\int_{|\Xi^{|}|=0}^{|\Xi^{|}|=\delta}\frac{1}{2}\,C\,|\Xi^{|}|\left[\boldsymbol{F} : [\hat{\Xi}^{|}\otimes\hat{\Xi}^{|}] - 1\right]^2|\Xi^{|}|\;\mathrm{d}\,|\Xi^{|}|\;\mathrm{d}\,\Theta^{|}\,, \tag{11}$$

that after some mathematical steps reduces to

$$\Psi = \frac{\pi}{48}\,C\,\delta^3\,[3\lambda^2 + 3\eta^2 + 2\lambda\eta - 8\lambda - 8\eta + 8]\,. \tag{12}$$

Finally, in order to obtain Poisson's ratio, we set $\delta\Psi = 0$ as explained before, see Eq. (5), resulting in

$$\frac{\partial\Psi}{\partial\nu}\doteq 0 \qquad \Rightarrow \qquad \frac{\partial\Psi}{\partial\eta}\frac{\partial\eta}{\partial\nu}\doteq 0 \qquad \Rightarrow \qquad \frac{\partial\Psi}{\partial\eta}\doteq 0\,. \tag{13}$$

Using the internal energy density (12), and setting its derivative with respect to η to zero furnishes

$$\frac{\partial\Psi}{\partial\eta} = \frac{\pi}{48}\,C\,\delta^3\,[6\eta + 2\lambda - 8]\doteq 0 \quad \Rightarrow \quad 6\eta + 2\lambda - 8\doteq 0 \quad \Rightarrow \quad 6[\eta - 1] + 2[\lambda - 1]\doteq 0\,, \tag{14}$$

that immediately transfers to

$$-\frac{\eta - 1}{\lambda - 1} = \frac{1}{3} \qquad \text{and since} \qquad \nu = \frac{1-\eta}{\lambda - 1} \qquad \Rightarrow \qquad \nu = \frac{1}{3}\,. \tag{15}$$

Therefore, our variational approach proves that for two-dimensional bond-based peridynamics, Poisson's ratio must be $\nu = \frac{1}{3}$ to retain equilibrium. One may infer that the obtained relation (15) renders the Poisson's ratio $\nu = \frac{1}{3}$ only according to the Biot definition. However, that is not true. With a little mathematical effort, and using L'Hopital's rule if necessary, it can be shown that in the vicinity of the reference configuration, the analysis leads to $\nu = \frac{1}{3}$ for all the canonical definitions of the nonlinear Poisson's ratio, as expected. That is

$$\begin{aligned}
&\text{Biot} \quad : \quad \nu = \frac{1-\eta}{\lambda-1} \quad , \quad \text{if } -\frac{\eta-1}{\lambda-1} = \frac{1}{3} \quad \Rightarrow \quad \nu = \frac{1}{3}\,,\\
&\text{Hencky} \quad : \quad \nu = -\frac{\ln\eta}{\ln\lambda} \quad , \quad \text{if } -\frac{\eta-1}{\lambda-1} = \frac{1}{3} \quad \Rightarrow \quad \nu = \frac{1}{3}\,,\\
&\text{Green} \quad : \quad \nu = \frac{1-\eta^2}{\lambda^2-1} \quad , \quad \text{if } -\frac{\eta-1}{\lambda-1} = \frac{1}{3} \quad \Rightarrow \quad \nu = \frac{1}{3}\,,\\
&\text{Almansi} \quad : \quad \nu = \frac{1-\eta^{-2}}{\lambda^{-2}-1} \quad , \quad \text{if } -\frac{\eta-1}{\lambda-1} = \frac{1}{3} \quad \Rightarrow \quad \nu = \frac{1}{3}\,.
\end{aligned} \tag{16}$$

2.2 Three-Dimensional Formulation

For a three-dimensional domain, the internal energy density Ψ per unit *volume* in the material configuration is the integral of its density $\psi^{|}$ over the horizon $\mathcal{H}_0$. That is, $\psi^{|}$ is the internal energy density per *volume* squared in the material configuration as

$$\begin{aligned} \psi^{\prime} &= \frac{1}{2} C L^{\prime} [S^{\prime} - 1]^2 \qquad \Rightarrow \\ \Psi &= \frac{1}{2} \int_{\mathcal{H}_0} \psi^{\prime} \, \mathrm{d} V^{\prime} \qquad \Rightarrow \\ \Psi &= \frac{1}{2} \int_{\mathcal{H}_0} \frac{1}{2} C L^{\prime} [S^{\prime} - 1]^2 \, \mathrm{d} V^{\prime} . \end{aligned} \tag{17}$$

Again, the factor one-half before the integral is introduced to prevent double-counting since the combination of each pair of points within the horizon occurs twice. For the uniaxial tension test of interest here, the internal energy density Ψ reads

$$\Psi = \frac{1}{2} \int_{\mathcal{H}_0} \frac{1}{2} C \, |\boldsymbol{\Xi}^{\prime}| \, \Big[\frac{|\boldsymbol{F} \cdot \boldsymbol{\Xi}^{\prime}|}{|\boldsymbol{\Xi}^{\prime}|} - 1 \Big]^2 \, \mathrm{d} V^{\prime} , \tag{18}$$

which in terms of the magnitude $|\boldsymbol{\Xi}^{\prime}|$ and the director $\hat{\boldsymbol{\Xi}}^{\prime}$ can be expressed as

$$\Psi = \frac{1}{2} \int_{\mathcal{H}_0} \frac{1}{2} C \, |\boldsymbol{\Xi}^{\prime}| \, \Big[|\boldsymbol{F} \cdot \hat{\boldsymbol{\Xi}}^{\prime}| - 1 \Big]^2 \, \mathrm{d} V^{\prime} \qquad \text{with} \qquad \boldsymbol{F} = \mathrm{Diag}(\lambda, \eta, \eta) . \tag{19}$$

Again, Eq. (19) is nonlinear with λ and η not necessarily close to one. However, in order to show how the current proposition recovers the established linear solution, we also provide its linearized version close to the reference configuration. Through linearization, see 1, the internal energy density Ψ reads

$$\begin{aligned} &\Psi = \frac{1}{2} \int_{\mathcal{H}_0} \frac{1}{2} C \, |\boldsymbol{\Xi}^{\prime}| \, \Big[\boldsymbol{F} : [\hat{\boldsymbol{\Xi}}^{\prime} \otimes \hat{\boldsymbol{\Xi}}^{\prime}] - 1 \Big]^2 \, \mathrm{d} V^{\prime} \qquad \text{with} \\ &\boldsymbol{F} = \mathrm{Diag}(\lambda, \eta, \eta) \qquad \text{and} \qquad \{\lambda, \eta\} \approx 1 . \end{aligned} \tag{20}$$

Integrating Eq. (20) over the horizon using a spherical coordinates system with $\mathrm{d} V^{\prime} = |\boldsymbol{\Xi}^{\prime}|^2 \sin \Phi^{\prime} \, \mathrm{d} \, |\boldsymbol{\Xi}^{\prime}| \, \mathrm{d} \, \Phi^{\prime} \, \mathrm{d} \, \Theta^{\prime}$ renders

$$\Psi = \frac{1}{2} \int_{\Theta^{\prime}=0}^{\Theta^{\prime}=2\pi} \int_{\Phi^{\prime}=0}^{\Phi^{\prime}=\pi} \int_{|\boldsymbol{\Xi}^{\prime}|=0}^{|\boldsymbol{\Xi}^{\prime}|=\delta} \frac{1}{2} C \, |\boldsymbol{\Xi}^{\prime}| \, \Big[\boldsymbol{F} : [\hat{\boldsymbol{\Xi}}^{\prime} \otimes \hat{\boldsymbol{\Xi}}^{\prime}] - 1 \Big]^2 \, |\boldsymbol{\Xi}^{\prime}|^2 \sin \Phi^{\prime} \, \mathrm{d} \, |\boldsymbol{\Xi}^{\prime}| \, \mathrm{d} \, \Phi^{\prime} \, \mathrm{d} \, \Theta^{\prime} , \tag{21}$$

that after some mathematical steps reduces to

$$\Psi = \frac{\pi}{60} C \, \delta^4 \, [3\lambda^2 + 8\eta^2 + 4\lambda\eta - 10\lambda - 20\eta + 15] . \tag{22}$$

Finally, in order to obtain Poisson's ratio, we set $\delta \Psi = 0$ resulting in

$$\frac{\partial \Psi}{\partial \nu} \doteq 0 \qquad \Rightarrow \qquad \frac{\partial \Psi}{\partial \eta} \frac{\partial \eta}{\partial \nu} \doteq 0 \qquad \Rightarrow \qquad \frac{\partial \Psi}{\partial \eta} \doteq 0 . \tag{23}$$

Using the internal energy density (22) and setting its derivative with respect to η to zero furnishes

$$\begin{aligned} \frac{\partial \Psi}{\partial \eta} &= \frac{\pi}{60} C \, \delta^4 \, [16\eta + 4\lambda - 20] \\ &\doteq 0 \quad \Rightarrow \quad 16\eta + 4\lambda - 20 \doteq 0 \quad \Rightarrow \quad 4[\eta - 1] + [\lambda - 1] \doteq 0 , \end{aligned} \tag{24}$$

that immediately transfers so

$$-\frac{\eta-1}{\lambda-1}=\frac{1}{4} \qquad \text{and since} \qquad \nu=\frac{1-\eta}{\lambda-1} \qquad \Rightarrow \qquad \nu=\frac{1}{4}\,. \tag{25}$$

Therefore, our variational approach proves that for three-dimensional bond-based peridynamics, Poisson's ratio must be $\nu=\frac{1}{4}$ to retain equilibrium. Again, the obtained relation (25) renders $\nu=\frac{1}{4}$ not only according to the Biot definition, but also for all the canonical definitions of the nonlinear Poisson's ratio, as expected. That is

$$\begin{aligned}
&\text{Biot} \quad : \quad \nu=\frac{1-\eta}{\lambda-1} \quad , \quad \text{if } -\frac{\eta-1}{\lambda-1}=\frac{1}{4} \quad \Rightarrow \quad \nu=\frac{1}{4}\,,\\
&\text{Hencky} \quad : \quad \nu=-\frac{\ln\eta}{\ln\lambda} \quad , \quad \text{if } -\frac{\eta-1}{\lambda-1}=\frac{1}{4} \quad \Rightarrow \quad \nu=\frac{1}{4}\,,\\
&\text{Green} \quad : \quad \nu=\frac{1-\eta^2}{\lambda^2-1} \quad , \quad \text{if } -\frac{\eta-1}{\lambda-1}=\frac{1}{4} \quad \Rightarrow \quad \nu=\frac{1}{4}\,,\\
&\text{Almansi} \quad : \quad \nu=\frac{1-\eta^{-2}}{\lambda^{-2}-1} \quad , \quad \text{if } -\frac{\eta-1}{\lambda-1}=\frac{1}{4} \quad \Rightarrow \quad \nu=\frac{1}{4}\,.
\end{aligned} \tag{26}$$

3 Results and Discussions

The goal of this section is to further explain the proposed approach through a series of examples, and to highlight the significance of introducing the notion of nonlinear Poisson's ratio to bond-based PD. For the discussions here, we include both two-dimensional and three-dimensional results side by side. Furthermore, the prescribed longitudinal stretch λ is not necessarily close to one. As we will see shortly, larger deformations can lead to Poisson's ratio other than $\frac{1}{3}$ for two-dimensional and other than $\frac{1}{4}$ for three-dimensional problems.

Figure 3 illustrates Poisson's ratio versus stretch for all the canonical definitions of Poisson's ratio. Poisson's ratio for each given λ is calculated via minimizing Ψ with respect to ν by setting $\partial\Psi/\partial\nu=0$ as explained previously. Note that in this graph, as well as all the other graphs in this section, the internal energy density Ψ is obtained using its nonlinear versions (9) and (19) for two-dimensional and three-dimensional calculations, respectively. The canonical definitions of the nonlinear Poisson's ratio are gathered. It can be clearly seen that all the definitions coincide at the reference configuration recovering $\nu=\frac{1}{3}$ and $\nu=\frac{1}{4}$ for two-dimensional and three-dimensional settings, respectively. Figure 3 also shows that Poisson's ratio is not constant, but it is a function of the prescribed stretch λ.

For the given range of λ in Fig. 3, the nonlinear Poisson's ratio according to Biot definition seems nearly constant; but we emphasize that it is not. Figure 4 shows the behavior of the Biot nonlinear Poisson's ratio for a larger range of λ clearly showing that Poisson's ratio can vary significantly if the deformations are not small.

So far, we have established that Poisson's ratio is obtained via minimizing the energy with respect to ν. Figures 5 and 6 illustrate the energy Ψ itself versus ν for various prescribed longitudinal stretches λ. The insets in each graph provide a zoomed window in the proximity of the solution where Ψ reaches its minimum. The nonlinear Poisson's ratio in these graphs follows the Biot definition. Nonetheless, a similar study can be carried out for all the other canonical definitions rendering similar results.

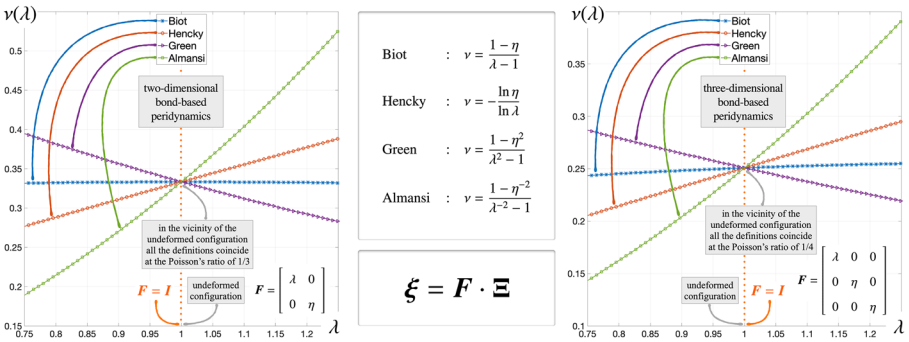

Fig. 3 Nonlinear Poisson's ratio ν versus longitudinal stretch λ for two-dimensional (left) and three-dimensional (right) problems. All the canonical definitions of Poisson's ratio coincide in the vicinity of the reference configuration, recovering $\nu = \frac{1}{3}$ and $\nu = \frac{1}{4}$ for two-dimensional and three-dimensional settings, respectively

Remark Note that the analysis here is generic and, in principle, valid also for any discrete system of lumped masses connected by springs. That is in all such systems, we expect a dependence of the Poisson's ratio on deformation, as soon as the deformations are no longer infinitesimal. In fact, we have indeed "verified" our derivations and conclusions via computational simulations using bond-based PD that exactly match our analytical solutions for the nonlinear behavior of Poisson's ratio. For the sake of brevity, and considering the analytical nature of the manuscript, we omit the discussion on the computational aspects and examples. Nonetheless, one can reproduce Figs. 5 and 6 using numerical simulations, too. Furthermore, the current analysis paves the way to investigate the behavior of Poisson's ratio, e.g., in state-based peridynamics [6] or continuum-kinematics-inspired peridynamics [7].

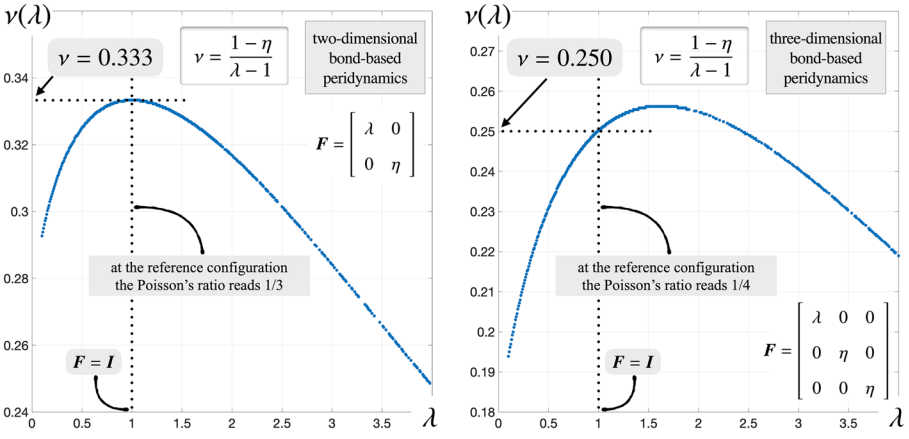

Fig. 4 Biot nonlinear Poisson's ratio ν versus longitudinal stretch λ for two-dimensional (left) and three-dimensional (right) problems. Poisson's ratio at the reference configuration, recovers $\nu = \frac{1}{3}$ and $\nu = \frac{1}{4}$ for two-dimensional and three-dimensional settings, respectively

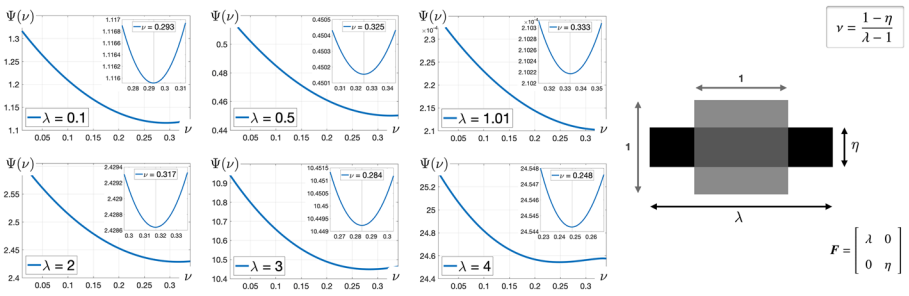

Fig. 5 Two-dimensional energy density Ψ versus the Biot nonlinear Poisson's ratio for various longitudinal stretches λ

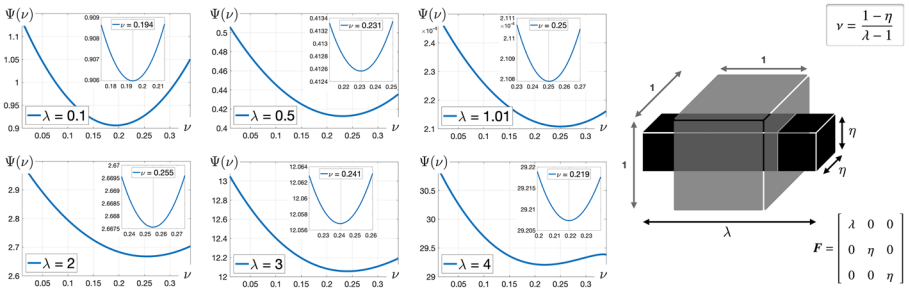

Fig. 6 Three-dimensional energy density Ψ versus the Biot nonlinear Poisson's ratio for various longitudinal stretches λ

4 Conclusion

Bond-based peridynamics, despite its restriction regarding Poisson's ratio, has been frequently employed to predict the behavior of materials, and in particular with application to damage and fracture. The presented study sheds light on the notion of Poisson's ratio in bond-based peridynamics and provides a geometrically exact description of the problem, resulting in a nonlinear Poisson's ratio. The nonlinear Poisson's ratio is not a constant and it can change significantly at large deformations. At the reference configuration though, the nonlinear Poisson's ratio coincides with $\nu = \frac{1}{3}$ for two-dimensional and $\nu = \frac{1}{4}$ for three-dimensional problems. We emphasize that the authors do not claim that the bond-based PD cannot be used for large elastic deformations. On the contrary, the manuscript shows that the bond-based PD has the potential to be employed for large nonlinear elastic deformations, albeit care should be taken when commenting about its Poisson's ratio if deformations are no longer infinitesimal. Apart from introducing the nonlinear Poisson's ratio to bond-based PD for the first time, a key feature of the current study is that the notions of "stress" and "strain" are entirely absent from the framework, as it is expected in a PD framework. We believe that this contribution can significantly enhance our understanding of the non-local behavior of materials using bond-based peridynamics at large deformations.

Linearization Procedure

The purpose of this Appendix is to show how the linearization of

$$\Psi = \frac{1}{2}\int_{\mathcal{H}_0} \frac{1}{2}\, C\, |\boldsymbol{\Xi}^{\shortmid}|\, \Big[\, |\boldsymbol{F}\cdot\hat{\boldsymbol{\Xi}}^{\shortmid}| - 1\,\Big]^2 \,\mathrm{d}\,A^{\shortmid} \qquad \text{with} \qquad \boldsymbol{F} = \mathrm{Diag}(\lambda,\eta)\,, \tag{27}$$

furnishes

$$\begin{aligned} &\Psi = \frac{1}{2}\int_{\mathcal{H}_0} \frac{1}{2}\, C\, |\boldsymbol{\Xi}^{\shortmid}|\, \Big[\, \boldsymbol{F} : [\hat{\boldsymbol{\Xi}}^{\shortmid}\otimes\hat{\boldsymbol{\Xi}}^{\shortmid}] - 1\,\Big]^2 \,\mathrm{d}\,A^{\shortmid} \qquad \text{with} \\ &\boldsymbol{F} = \mathrm{Diag}(\lambda,\eta) \qquad \text{and} \qquad \{\lambda,\eta\} \approx 1\,. \end{aligned} \tag{28}$$

In doing so, we begin with the fact that

$$|\boldsymbol{F}\cdot\hat{\boldsymbol{\Xi}}^{\shortmid}| = \frac{\xi^{\shortmid}}{\Xi^{\shortmid}}\,, \tag{29}$$

for which, the linearization yields

$$\mathrm{Lin}\ \frac{\xi^{\shortmid}}{\Xi^{\shortmid}} = \frac{\xi^{\shortmid}}{\Xi^{\shortmid}}\bigg|_{\boldsymbol{F}=\mathbb{I}} + \frac{\partial}{\partial\boldsymbol{F}}\left(\frac{\xi^{\shortmid}}{\Xi^{\shortmid}}\right)\bigg|_{\boldsymbol{F}=\boldsymbol{I}} : \big[\boldsymbol{F}-\boldsymbol{I}\big]\,. \tag{30}$$

At the reference configuration, the first term reduces to unity as

$$\frac{\xi^{\shortmid}}{\Xi^{\shortmid}}\bigg|_{\boldsymbol{F}=\boldsymbol{I}} = \frac{\|\boldsymbol{F}\cdot\boldsymbol{\Xi}^{\shortmid}\|}{\Xi^{\shortmid}}\bigg|_{\boldsymbol{F}=\boldsymbol{I}} = \frac{\|\boldsymbol{I}\cdot\boldsymbol{\Xi}^{\shortmid}\|}{\Xi^{\shortmid}} = \frac{\Xi^{\shortmid}}{\Xi^{\shortmid}} = 1\,. \tag{31}$$

Next, the derivative of $\xi^{\shortmid}/\Xi^{\shortmid}$ with respect to $\boldsymbol{F}$ is evaluated as

$$\frac{\partial}{\partial\boldsymbol{F}}\left(\frac{\xi^{\shortmid}}{\Xi^{\shortmid}}\right) = \frac{1}{\Xi^{\shortmid}}\frac{\partial\xi^{\shortmid}}{\partial\boldsymbol{F}} = \frac{1}{\Xi^{\shortmid}}\frac{\partial\xi^{\shortmid}}{\partial\boldsymbol{\xi}^{\shortmid}}\cdot\frac{\partial\boldsymbol{\xi}^{\shortmid}}{\partial\boldsymbol{F}} \qquad \text{with} \qquad \frac{\partial\boldsymbol{\xi}^{\shortmid}}{\partial\boldsymbol{F}} = \boldsymbol{i}\otimes\boldsymbol{\Xi}^{\shortmid}\,, \tag{32}$$

where $\boldsymbol{i}$ is the identity tensor. Thus,

$$\frac{\partial}{\partial\boldsymbol{F}}\left(\frac{\xi^{\shortmid}}{\Xi^{\shortmid}}\right) = \frac{1}{\Xi^{\shortmid}}\frac{\partial\xi^{\shortmid}}{\partial\boldsymbol{\xi}^{\shortmid}}\cdot\big[\boldsymbol{i}\otimes\boldsymbol{\Xi}^{\shortmid}\big] = \frac{1}{\Xi^{\shortmid}}\frac{\boldsymbol{\xi}^{\shortmid}}{\xi^{\shortmid}}\cdot\big[\boldsymbol{i}\otimes\boldsymbol{\Xi}^{\shortmid}\big]\,. \tag{33}$$

This expression, evaluated at $\boldsymbol{F}=\boldsymbol{I}$ returns

$$\frac{\partial}{\partial\boldsymbol{F}}\left(\frac{\xi^{\shortmid}}{\Xi^{\shortmid}}\right)\bigg|_{\boldsymbol{F}=\boldsymbol{I}} = \frac{1}{\Xi^{\shortmid}}\frac{\partial\Xi^{\shortmid}}{\partial\boldsymbol{\Xi}^{\shortmid}}\cdot\big[\boldsymbol{I}\otimes\boldsymbol{\Xi}^{\shortmid}\big] = \frac{1}{{\Xi^{\shortmid}}^2}\boldsymbol{\Xi}^{\shortmid}\otimes\boldsymbol{\Xi}^{\shortmid} = \frac{\boldsymbol{\Xi}^{\shortmid}}{\Xi^{\shortmid}}\otimes\frac{\boldsymbol{\Xi}^{\shortmid}}{\Xi^{\shortmid}} = \hat{\boldsymbol{\Xi}}^{\shortmid}\otimes\hat{\boldsymbol{\Xi}}^{\shortmid}\,. \tag{34}$$

Finally, plugging this and Eq. (31) in the initial expression (30) yields

$$\mathrm{Lin}\ \frac{\xi^{\shortmid}}{\Xi^{\shortmid}} = 1 + \big[\hat{\boldsymbol{\Xi}}^{\shortmid}\otimes\hat{\boldsymbol{\Xi}}^{\shortmid}\big] : \big[\boldsymbol{F}-\boldsymbol{I}\big] = 1 + \big[\hat{\boldsymbol{\Xi}}^{\shortmid}\otimes\hat{\boldsymbol{\Xi}}^{\shortmid}\big] : \boldsymbol{F} - \hat{\boldsymbol{\Xi}}^{\shortmid}\cdot\hat{\boldsymbol{\Xi}}^{\shortmid} \qquad \text{with} \qquad \hat{\boldsymbol{\Xi}}^{\shortmid}\cdot\hat{\boldsymbol{\Xi}}^{\shortmid} = 1\,, \tag{35}$$

or simply

$$\text{Lin } \frac{\underline{\xi}^{\shortmid}}{\underline{\Xi}^{\shortmid}} = \left[\hat{\underline{\Xi}}^{\shortmid} \otimes \hat{\underline{\Xi}}^{\shortmid}\right] : \boldsymbol{F}. \tag{36}$$

Acknowledgements The authors gratefully acknowledge the support provided by the Scientific and Technological Research Council of Turkey (TÜBITAK) Career Development Program, grant number 218M700.

Declarations

Conflicts of Interest On behalf of all authors, the corresponding author states that there is no conflict of interest.

References

1. Silling S (2000) Reformulation of elasticity theory for discontinuities and long-range forces. J Mech Phys Solids 48(1):175–209
2. Dell'Isola F, Andreaus U, Placidi L (2015) At the origins and in the vanguard of peridynamics, non-local and higher-gradient continuum mechanics: An underestimated and still topical contribution of Gabrio Piola. Math Mech Solids 20(8):887–928
3. Madenci E, Oterkus E (2014) Peridynamic theory and its applications, Springer
4. Javili A, Morasata R, Oterkus E, Oterkus S (2019) Peridynamics Review. Math Mech Solids 24:3714–3739
5. Silling SA, Epton M, Weckner O, Xu J, Askari E (2007) Peridynamic states and constitutive modeling. J Elast 88(2):151–184
6. Silling SA, Lehoucq RB (2010) Peridynamic theory of solid mechanics. Adv Appl Mech 44:73–168
7. Javili A, McBride AT, Steinmann P (2019) Continuum-kinematics-inspired peridynamics. Mechanical problems. J Mech Phys Solids 131:125–146
8. Gerstle W, Sau N, Silling S (2005) Peridynamic modeling of plain and reinforced concrete structures, In: 18th international conference on structural mechanics in reactor technology (SMiRT 18) 54–68
9. Trageser J, Seleson P (2020) Bond-based peridynamics: a tale of two poisson ratios. Journal of Peridynamics and Nonlocal Modeling 2:278–288
10. Beatty MF, Stalnaker DO (1986) The poisson function of finite elasticity. Journal of Applied Mechanics, Transactions ASME 53(4):807–813
11. Mihai LA, Budday S, Holzapfel GA, Kuhl E, Goriely A (2017) A family of hyperelastic models for human brain tissue. J Mech Phys Solids 106:60–79
12. Bakiler AD, Javili A (2020) Bifurcation behavior of compressible elastic half-space under plane deformations. Int J Non-Linear Mech 126